Desalination and Water Treatment
www.deswater.com

doi:10.5004/dwt.2018.21899

103 (2018) 175–181
January

Green synthesis of 3D porous graphene/lignin composites with improved adsorption capacity for heavy metal ions in aqueous solution

Fang Zhou, Jingang Yu, Xinyu Jiang*

School of Chemistry and Chemical Engineering, Central South University, Changsha 410083, China, email: 346817616@qq.com (F. Zhou), yujg@csu.edu.cn (J. Yu), jiangxinyu@csu.edu.cn (X. Jiang)

Received 28 July 2017; Accepted 4 January 2018

ABSTRACT

Lignin modified three-dimensional porous graphene (denoted as 3D PG/L) were synthesized via a green hydrothermal and freeze-drying method. The as-prepared 3D PG-L was characterized by scanning electron microscopy, transmission electron microscopy, Fourier transform infrared spectroscopy, thermo-gravimetric analysis, X-ray photoelectron spectroscopy and N_2 adsorption-desorption measurements. A series of adsorption experiments for heavy metal ions were used to investigate the effects of lignin on the graphene structure. It was found that 3D PG-L showed a significant increase in oxygen-containing groups and adsorption capacity contrast to 3D PG. These impressive results demonstrated that the as-prepared porous composites achieved the improved adsorption capacity for heavy metal ions from an aqueous solution. The results indicated that the adsorption process matched well with the Langmuir isotherm model and the pseudo-second-order kinetic model. This study provides a novel functional 3D porous graphene as adsorbent for the removal of heavy metal ions from an aqueous solution.

Keywords: Three-dimensional porous graphene; Lignin; Composite materials; Metal ions; Adsorption

1. Introduction

Three-dimensional porous graphene (3D PG) have been widely applied in super-capacitors, batteries, and nanocarrier [1–3], which exhibit large surface area, continuously interconnected porous structure and high electrical conductivity. 3D porous graphene-based frame works also have an increasing number of applications in the area of new materials. Similarly, the porous carbon materials exhibit excellent performance in environmental concerns, including dye and heavy metal ions adsorption [4,5]. The contaminants in geochemical systems whether inorganic metal ions or organic dyes are quite harmful to human and other life [6,7]. The disposal of an increased discharged wastewater containing heavy metal ions is one of the most serious environment problems in the modern life. It is significative to explore novel materials for the efficient removal heavy metal ions, which are not biodegradable [8]. Experimental investigations suggested that modified 3D PG materials are regarded as an ideal candidate of the excellent adsorbent for water purification [9]. Previous studies developed several modification methods to exploit deeply potentiality of 3D PG, such as doping graphene with heteroatom [2,10], incorporating with biocompatible polymer [3], introducing with functional groups [11,12].

Lignin is an available and heterogeneous biopolymer to modify 3D PG, due to the highly-branched and three-dimensional structures [13]. Lignin is composed of three different phenylpropanoid subunits, namely, sinapyl alcohols, p-coumaryl and coniferyl [14]. Specifically, lignin provides with various oxygen groups, including many hydroxyl, aromatic methoxyl, carbonyl, and carboxyl [15]. Because of increasingly requirement for removal of metal ions, lignin is an ideal candidate incorporating graphene to improve biocompatibility and adsorption ability [16,17]. Furthermore, lignin provides more oxygen-containing functional groups and adsorption sites [18]. It is suitable for a wide range of advanced applications, including drug delivery, detection of heavy metal ions and chemical adsorption. However, the

*Corresponding author.

lignin modified three-dimensional graphene for pollutants removal has been hardly reported.

In this paper, a green-synthesis functional 3D PG was prepared by a one-step hydrothermal and freeze-drying method with the assistance of lignin. . In contrast to other methods, such as chemical activation, annealing and inclusion of templates; the facile hydrothermal method is more efficient and environmental [19]. Moreover, some unique features could be retained, such as good dispersibility in water or a propensity to self-assemble into monolithic gels under hydrothermal treatment. The as-prepared material was characterized by various analytical methods, which was expected to combine the advantages of ease of preparation and excellent metal ions absorbing ability. In addition, the applications of 3D porous graphene/lignin (PG/L) for the removal of Cd(II) and Pb(II) from an aqueous solution were investigated by adsorption experiments. The adsorption kinetics and isotherms were also analyzed by interpreting the experimental data. Moreover, the characterization and adsorption results were used to evaluate the influences of lignin on the morphology, structure and adsorption ability of 3D PG.

2. Experimental

2.1. Materials

Natural flaky graphite (purity >90%) was purchased from Shenzhen Nanotech Port Co., Ltd. Lignin was obtained from Tianjin Guangfu Fine Chemical Research Institute. All chemical reagents were of analytical grade and used as received without any further treatment. Ultra-pure water was produced using a Milli-Q water purification system (Millipore, Milford, MA).

2.2. Pretreatment of graphene oxide (GO)

Graphene oxide (GO) was obtained by a modified Hummers method. Briefly, a mixture of natural flaky graphite (300 mg) and $KMnO_4$ (1.5 g) was placed in a flask, which was then cooled using an ice bath. Next, 40 mL of mixed acid, containing concentrated sulfuric acid and phosphoric acid (9:1, v/v), was slowly added dropwise. Then, this reaction system was transferred to an oil bath and stirred continuously for 12 h to introduce oxygen groups onto the graphene surface. The mixture was cooled with ice cubes and 20 mL of 30% H_2O_2 solution was added to reduce any remaining $KMnO_4$. A brilliant yellow dispersion was obtained, which was then washed with a 1 mol/L HCl aqueous solution three times to remove metal ions. Finally, the remaining salt was separated by centrifugation with ultra-pure water until a neutral pH was reached.

2.3. Prepration of 3D porous graphene/lignin composites (PG/L)

3D porous graphene/lignin composites (PG/L) were prepared from hydrothermal self-assembly in a homogeneous aqueous mixture of GO (5.5 mg/L) and lignin, followed by a freeze-drying process. Specifically, 20 mL GO suspension and 100 mg lignin were added into a breaker and treated with sonication for several minutes until a homogeneous dispersion was formed. Then, the mixture was transferred into a 25 mL Teflon-lined stainless-steel autoclave and maintained at 180°C for 1 h. Upon completion of the hydrothermal reaction, a three-dimensional graphene hydrogel column was obtained by freeze-drying for 48 h [20].

2.4. Characterizations

The morphology and composition of 3D PG and 3D PG/L were characterized with a field emission scanning electron micro-scopes (SEM, TESCAN MIRA3 LMH/LMU) and X-ray photoelectron spectroscopy (XPS, ESCALab220i-XL, VG Scientific), using Al K_α as the X-ray source. Thermogravimetric analysis (TGA, NETZSCH STA 449C) and Fourier transform infrared spectroscopy (FT-IR, Nicolet 6700) measurements were performed. The specific surface areas and porous microstructures of the materials were analyzed with N_2 adsorption-desorption measurements and Barrett-Emmett-Joyner-Halenda (BJH) method.

2.5. Adsorption experiments

Batch adsorption experiments were conducted to investigate the adsorption capacity of 3D PG/L on heavy metal ions. Briefly, 5.0 mg of adsorbent and 20.0 mL of Pb (II) and Cd (II) solution with different concentrations were added to 50 mL flask, respectively, which were shaken in a thermostat shaker for a certain amount of time. After filtration, the residual concentration of metal ions and the adsorption capacities were determined by ICP and calculated with Eq. (1):

$$q_e = \frac{(C_0 - C_e) \times V}{m} \tag{1}$$

where C_o and C_e (mg/L) are initial and equilibrium concentrations of Pb(II), respectively, m (mg) is the mass of the absorbent, V (L) is the volume of the solution, and q_e (mg/g) is the adsorption capacity of metal ions. All the experimental data were the averages of triplicate determinations and the relative error of the data were about 5%.

Adsorption kinetic experiments were carried out to determine the equilibrium time and adsorption rate. The equilibrium sorption experiments were performed to assess the metal ions uptake capacity of the as-prepared materials. Definitely, 5.0 mg of adsorbent was weighted into the flasks with 20.0 mL of metal ions solution (C_0 = 10–100 mg/L, 25°C, pH 6). To further investigate the mechanism of adsorption, most commonly theoretical models were employed to interpret the experimental data.

The adsorption kinetic models, pseudo-first-order and pseudo-second-order [21,22] can be expressed with Eqs. (2) and (3), respectively.

$$\ln(q_e - q_t) = \ln q_e - \frac{k_1}{2.303} t \tag{2}$$

$$\frac{t}{q_t} = \frac{1}{k_2 q_e^2} + \frac{1}{q_e} t \tag{3}$$

The adsorption isotherms models, Langmuir isotherm and Freundlich isotherm [23,24] can be presented with Eqs. (4) and (5), respectively.

$$\frac{c_e}{q_e} = \frac{c_e}{q_m} + \frac{1}{q_m k_d} \tag{4}$$

$$\ln q_e = \ln k_f + \frac{1}{n} \ln c_e \tag{5}$$

where q_t is the adsorption capacity at a certain time (mg/g), k_1 (1/min) and k_2 (g/mg·min) is the rate constant in the kinetic model; q_m is the maximum adsorption capacity (mg/g), k_d and k_f is the equilibrium constant of Langmuir and Freundlich isotherm, and $1/n$ is a heterogeneity measurement of the adsorption sites and an indicator of isotherm nonlinearity.

3. Results and discussion

3.1. Characterization of 3D PG/L

Fig. 1 shows the morphology and microstructure of 3D PG and 3D PG/L by means of SEM and TEM. As shown in Figs. 1a,b, the typical SEM images confirm the presence of three-dimensional interconnected frame works including macroporous structure. The SEM image of 3D PG/L (Fig. 1b) clearly reveals relatively rough surface morphology due to the presence of heterogeneous lignin. Remarkably, high-resolution TEM images (Figs. 1c,d) reveal that thread-like lignin was homogeneously distributed. Compared with single and sheet-like structure of 3D PG (Fig. 1c), three-dimensional lignin was homogeneously grown on functional 3D PG (Fig. 1d).

Representative nitrogen adsorption-desorption isotherms of 3D PG and 3D PG/L are shown in Fig. 2, and both curves are very similar to typical IV isotherms. The specific surface area of 3D PG-L (234.4 $m^2 g^{-1}$) is lower than that of 3D PG (262.4 $m^2 g^{-1}$), which might attribute to lignin partial occupation of the surface. Furthermore, the pore size distribution calculated by BJH methods demonstrated the existence of massive mesopores with average sizes of 3.055 nm (3D PG) and 1.87 nm (3D PG/L), respectively. Combined with the SEM and TEM images, these results preliminary suggest the success of 3D porous graphene / lignin synthesis.

FT-IR spectra of 3D PG and 3D PG/L are presented in Fig. 3. The absorption peaks at 3430 cm^{-1}, 1708 cm^{-1}, 1577 cm^{-1}, 1159 cm^{-1} and 1042 cm^{-1} are assigned as typical indication of vibration of O-H group, C=O group, C=C group, C-O-C group and C-O group, respectively. The as-prepared materials show similar spectral patterns, but differ from peak width and intensity.

To assess the reduction effect, Fig. 4 presents the TGA curves of 3D PG and 3D PG-L. The TGA curves show a

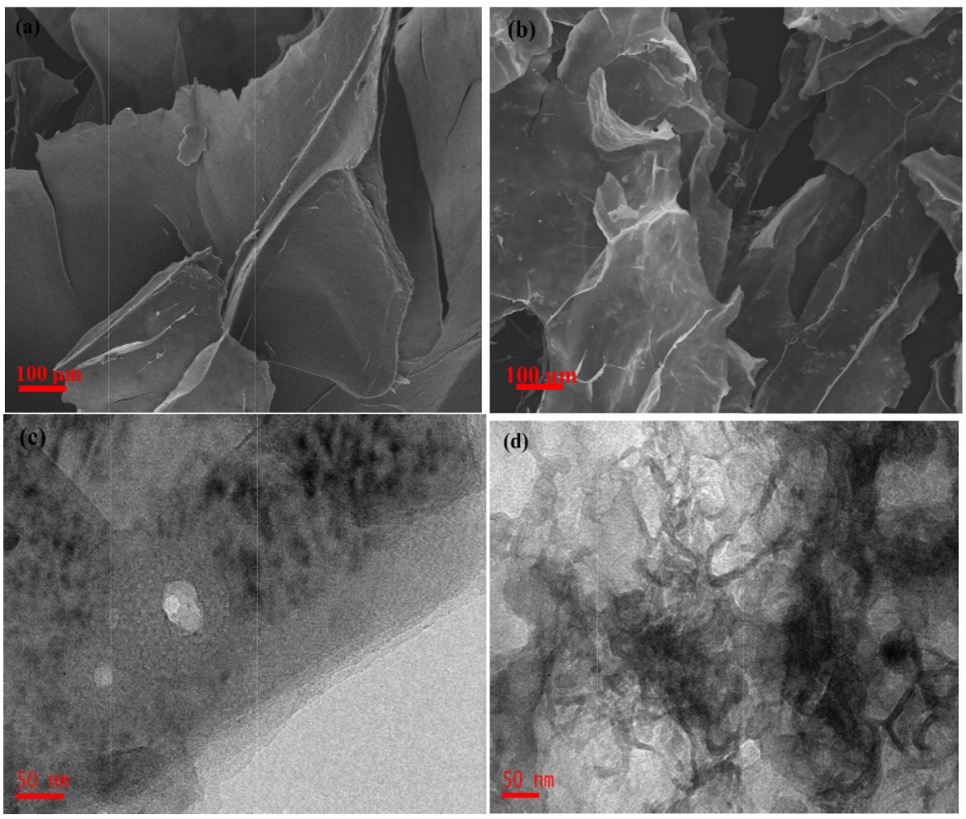

Fig. 1. SEM images of (a) 3D PG, (b) 3D PG/L; TEM images of (c) 3D PG, (d) 3D PG/L.

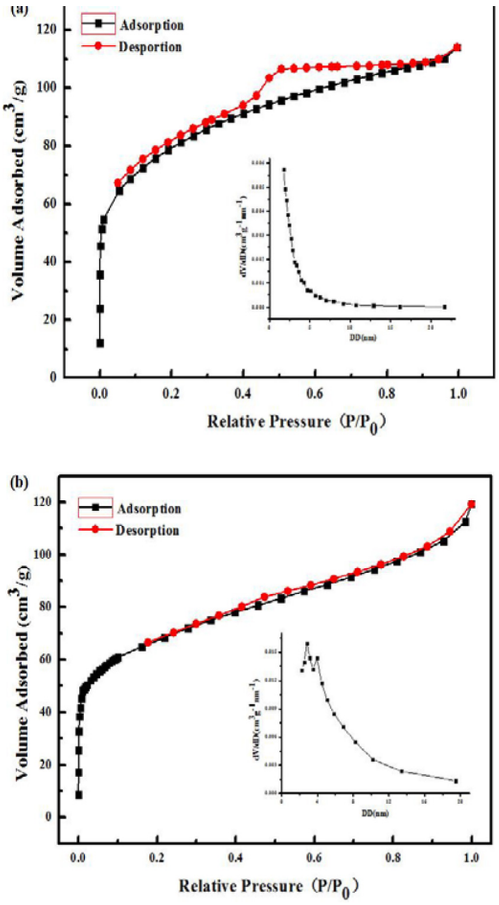

Fig. 2. N_2 adsorption-desorption isotherms and BJH pore distribution (inset) of (a) 3D PG and (b) 3D PG/L.

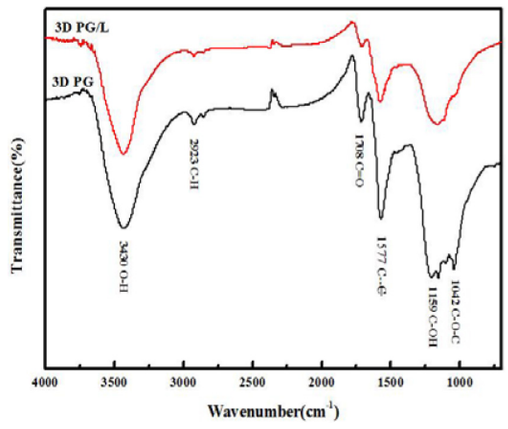

Fig. 3. IR spectra of 3D PG and 3D PG/L.

simple process due to the oxygen-containing functional groups covalently bound to 3D PG. Compared with 3D PG, 3D PG/L exhibited most obvious weight loss at a relatively higher temperature. It shows a significant stage for mass loss, which can be attributed to the thermal decomposition of the oxygen functional groups [25]. Furthermore, the oxygen contents increased from 54% for 3D PG to 74% for 3D PG/L, suggesting a decrease in the degree of reduction with assistance of lignin.

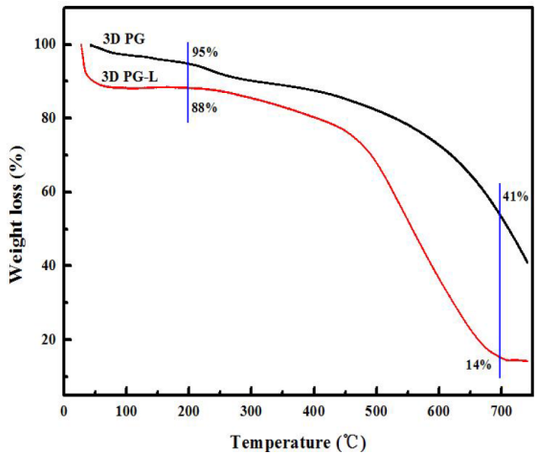

Fig. 4. TGA curves of 3D PG and 3D PG/L at a heating rate of 10 °C min^{-1} under the atmosphere of argon.

XPS survey was used to access the purity and functionality of as-prepared materials. Fig. 5a shows strong peaks at 284.8 and 532.5 eV corresponding to C1s and O1s. Particularly, C/O atomic ratios of 3D PG and 3D PG/L are 4.91 and 3.77, respectively [26]. Fig. 5b shows the high-resolution O1s spectrum and the peak of 3D PG/L is higher than that of 3D PG. The lower C/O atomic ratio and higher oxygen-rich functional groups of 3D PG/L indicate the insertion of some oxygen-containing functional groups with the assistance of lignin during the hydrothermal treatment process.

3.2. Adsorption test

Fig. 6 shows the adsorption test of 3D PG and 3D PG/L on the removal of Cu(II), Cd(II) and Pb(II) from aqueous solution. The maximum adsorption capacities of 3D PG-L were calculated to be about 43, 41 and 133 mg/g for Cu(II), Cd(II) and Pb(II), respectively. In contrast, the adsorption capacities of 3D PG were 36, 26 and 114 mg/g for the above three metal ions, respectively. Interestingly, the adsorption capacity of functional 3D PG toward metal ions was enhanced with the assistance of lignin. The high adsorption capacities toward metal ions might be attributed to the excellent complexation between oxygen-containing functional groups on the surface of adsorbent and metal ions. This is likely to refer to the importance of the amount of oxygen-containing functional groups on the surface of adsorbent, while above characterization analysis demonstrated that 3D PG-L showed a significant increase in oxygen-containing groups contrast to 3D PG. The presence of lignin effectively improved the metal ions adsorption capacity, which agreed well with the characterization results of 3D PG and 3D PG/L.

3.3. Adsorption kinetics

After the adsorption test, the 3D PG/L showed superior adsorption capacity compared to 3D PG, which was used for the deep investigation of the adsorption process. In con-

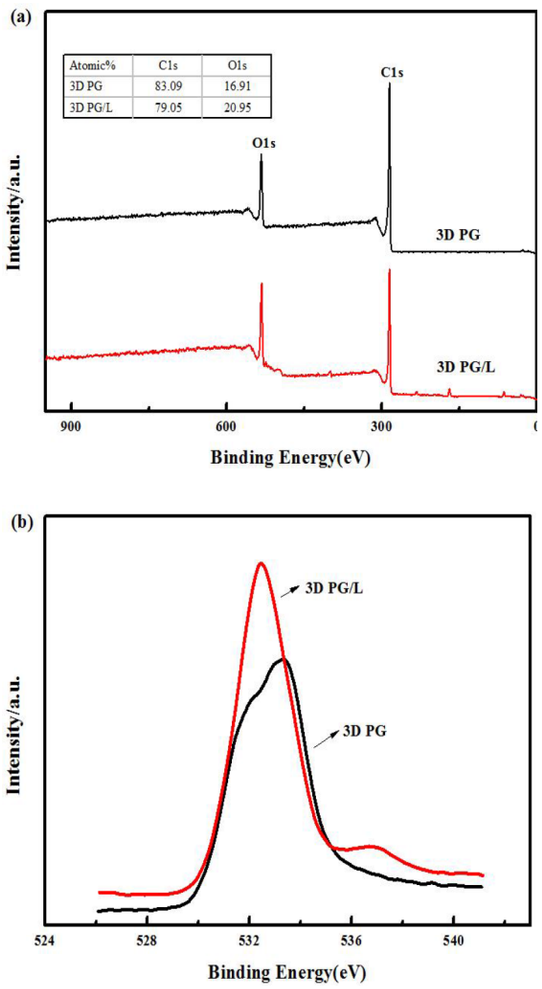

Fig. 5. (a) XPS survey and Atomic percentage (inset) of 3D PG and 3D PG/L; (b) O1s spectra of 3D PG and 3D PG/L.

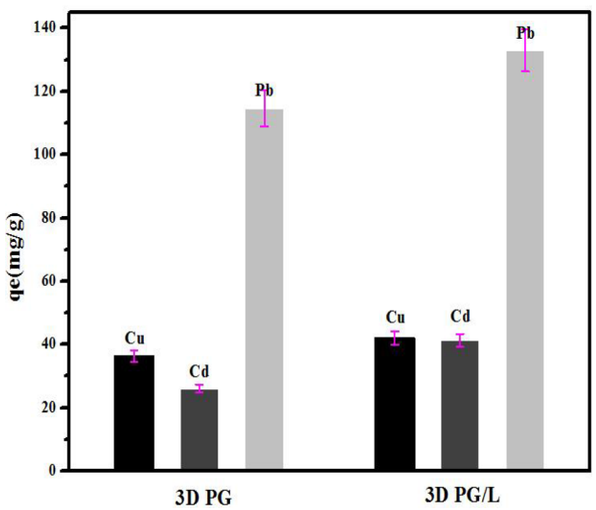

Fig. 6. Adsorption differences of Cd^{2+}, Pb^{2+} and Cd^{2+} on 3D PG and 3D PG/L.

trol experiments, Fig. 7 displays the adsorption behaviors of 3D PG/L towards Pb(II). Obviously, Fig. 7a shows that the adsorption occurred very fast initially, and the adsorption proceeded rapidly before reaching an equilibrium state after 70 min. The high adsorption rate within the 5 min was attributed to the large number of available adsorption sites.

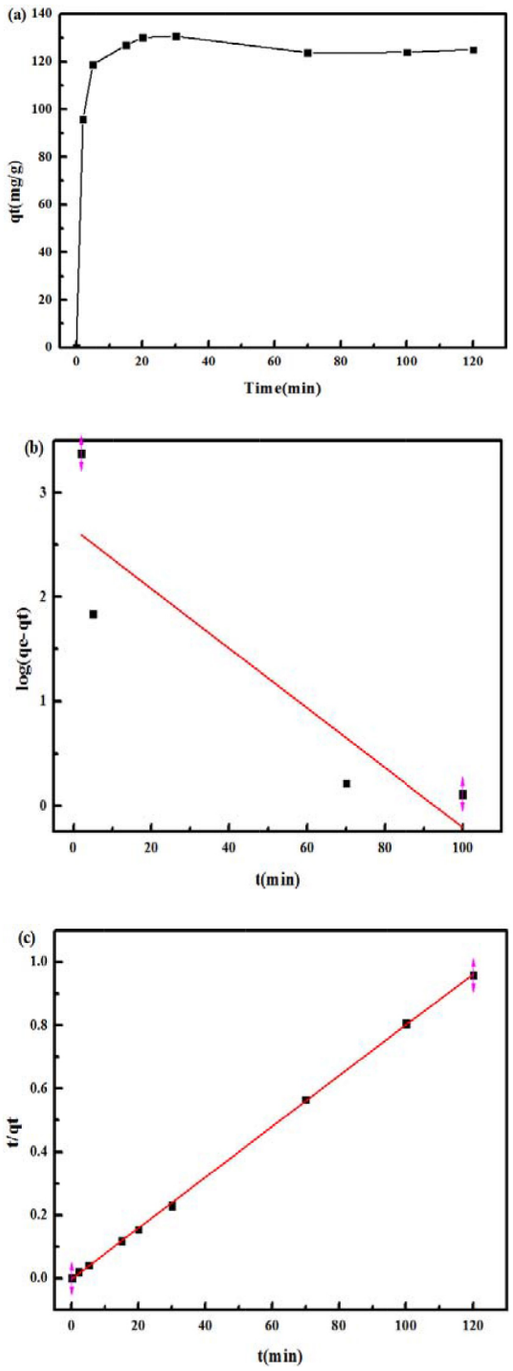

Fig. 7. (a) Effect of time on adsorption of Pb^{2+} by 3D PG/L; (b) Pseudo-first-order kinetic model; (c) Pseudo-second-order kinetic model.

Table 1
Kinetic parameters for the adsorption of Pb^{2+}

Equations	Parameters	3D PG/L
First-order-kinetic	q_m (mg/g)	14.17
	k_1 (min^{-1})	0.066
	R^2	0.716
Second-order-kinetic	q (mg/g)	124.5
	k_2 (min)	0.048
	R^2	0.999

To further investigate the mechanism of the adsorption, adsorption kinetic studies were interpreted as following. Table 1 provides the related kinetic parameters and correlation coefficients. The correlation coefficients (R^2) for the pseudo-first-order model (Fig. 7b, $R^2 = 0.716$) is relatively lower than the pseudo-second-order model (Fig. 7c, $R^2 = 0.999$). Meanwhile, the calculated results of the adsorption capacity of the pseudo-second-order (124.5 mg/g) is in good agreement with the experimental data (128.6 mg/g). It suggests that kinetic adsorptions are suitable for pseudo-second-order model.

3.4. Adsorption thermodynamics

Equilibrium adsorption isotherms are usually used to determine the capacities of adsorbents. Fig. 8a shows the adsorption isotherms of PG/L composites toward Pb(II) at 25°C and pH 6. The adsorption capacity increased with increasing equilibrium concentration, which is fitted well by Langmuir isotherm model (Fig. 8b). As presented in Table 2, Langmuir isotherm and Freundlich isotherm models were applied to fitting adsorption data. The saturation adsorption capacity (q_m) were calculated to be about 135.69 mg/g for Pb(II). Clearly, the adsorption of metal ions on 3D PG/L is more inclined to Langmuir isotherm ($R^2 > 0.99$) rather than Freundlich isotherm ($R^2 < 0.99$), suggesting a homogeneous and monolayer adsorption process.

3.5. Adsorption mechanisms

Based on the above experimental results, the main adsorption mechanisms of 3D PG/L composites are as followings: (i) The properties of the functional groups (oxygen functional groups) should be considered as important impacting factors to the adsorption, which is mainly attributed to the excellent complexation between oxygen-containing functional groups on the surface of adsorbent and metal ions. (ii) According to the theory of hard and soft acids and bases (HSAB) [27], the functional groups containing hydroxyl are considered to be soft base, and the heavy metal ions like Pb(II), Cu(II) and Cd(II) are considered to be soft acids, so the lignin functionalized 3D PG can be used to remove Pb(II), Cu(II) and Cd(II) from aqueous solution. (iii) The integrating mesopores into macroporous frameworks improve the adsorption capacity. It is certainly that the more precisely characte-

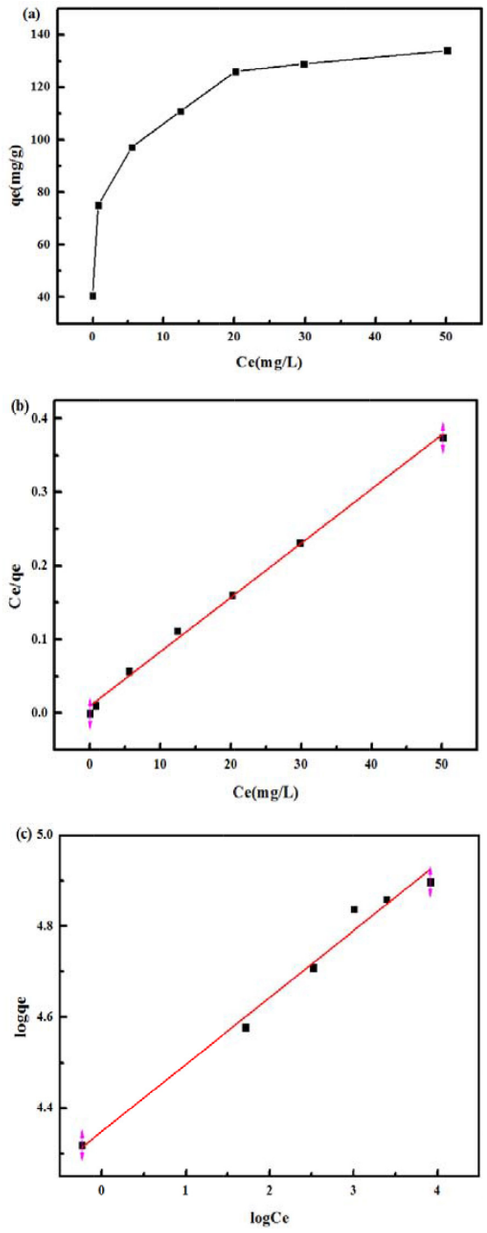

Fig. 8. (a) Adsorption isotherms of Pb^{2+} by 3D PG/L; (b) Langmuir model; (c) Freundlich model.

Table 2
Fitting results with Langmuir and Freundlich isotherm for Pb^{2+}

Equations	Parameters	3D PG/L
Langmuir isotherm	q_m (mg/g)	135.69
	b	0.75
	R^2	0.997
Freundlich isotherm	n	6.802
	k	77.437
	R^2	0.981

rization for the understanding of the adsorption mechanisms in detail are needed.

4. Conclusion

3D PG/L composites were successfully synthesized via a green hydrothermal self-assembly method with assistance of lignin. Using various characterization methods, the mesoporous structure was shown to be well integrated into the 3D macroscopic graphene-based structure. The as-prepared material was a novel modified three-dimensional porous graphene and used as adsorbent for removing heavy metal ions from aqueous solutions. Due to the lignin-assistant hydrothermal treatment, 3D PG/L showed obviously enhanced adsorption ability for removing Pb (II) and Cd (II). Adsorption kinetic and isotherm processes for Pb(II) were found to correlate with pseudo-second-order model and Langmuir isotherm model, respectively. This study provided a promising adsorbent for the removal of heavy metal ions from aqueous solution.

Acknowledgements

This work was supported by the National Natural Science Foundation of China (No. 21571191 and No. 51674292) and Provincial Natural Science Foundation of Hunan (2016JJ1023).

References

[1] H. Deng, L. Yao, Q.A. Huang, Q. Su, J. Zhang, G. Du, Highly improved electrochemical performance of Li-S batteries with heavily nitrogen-doped three-dimensional porous graphene interlayers, Mater. Res. Bull., 84 (2016) 218–224.

[2] D. Liu, C. Fu, N. Zhang, H. Zhou, Y. Kuang, Three-dimensional porous nitrogen doped graphene hydrogel for high energy density supercapacitors, Electrochim. Acta, 213 (2016) 291–297.

[3] H. Mianehrow, R. Afshari, S. Mazinani, F. Sharif, M. Abdouss, Introducing a highly dispersed reduced graphene oxide nano-biohybrid employing chitosan/hydroxyethyl cellulose for controlled drug delivery, Int. J. Pharm., 509 (2016) 400–407.

[4] X. Liu, J. Li, X. Wang, C. Chen, X. Wang, High performance of phosphate-functionalized graphene oxide for the selective adsorption of U(VI) from acidic solution, J. Nucl. Mater., 466 (2015) 56–64.

[5] L. Mahmoudian, A. Rashidi, H. Dehghani, R. Rahighi, Single-step scalable synthesis of three-dimensional highly porous graphene with favorable methane adsorption, Chem. Eng. J., 304 (2016) 784–792.

[6] X. Zou, Y. Yin, Y. Zhao, D. Chen, S. Dong, Synthesis of ferriferrous oxide/l-cysteine magnetic microspheres and their adsorption capacity for Pb (II) ions, Mater. Lett., 150 (2015) 59–61.

[7] Z. Wang, X. Zhang, X. Wu, J.-G. Yu, X.-Y. Jiang, Z.-L. Wu, X. Hao, Soluble starch functionalized graphene oxide as an efficient adsorbent for aqueous removal of Cd (II): The adsorption thermodynamic, kinetics and isotherms, J. Sol-Gel Sci. Technol., 82 (2017) 440–449.

[8] T. Gao, J. Yu, Y. Zhou, X. Jiang, The synthesis of graphene oxide functionalized with dithiocarbamate group and its prominent performance on adsorption of lead ions, J. Taiwan Inst. Chem. Eng., 71 (2017) 426–432.

[9] Y.C. Shi, A.J. Wang, X.L. Wu, J.R. Chen, J.J. Feng, Green-assembly of three-dimensional porous graphene hydrogels for efficient removal of organic dyes, J. Colloid. Interface. Sci., 484 (2016) 254–262.

[10] G. Li, J. Sun, W. Hou, S. Jiang, Y. Huang, J. Geng, Three-dimensional porous carbon composites containing high sulfur nanoparticle content for high-performance lithium-sulfur batteries, Nat. Commun., 7 (2016) 10601.

[11] F. Zhang, Y. Tang, H. Liu, H. Ji, C. Jiang, J. Zhang, X. Zhang, C.-S. Lee, Uniform Incorporation of Flocculent molybdenum disulfide nanostructure into three-dimensional porous graphene as an anode for high-performance lithium ion batteries and hybrid supercapacitors, ACS Appl. Mater .Interfaces, 8 (2016) 4691–4699.

[12] L. Sun, L. Lu, Y. Bai, K. Sun, Three-dimensional porous reduced graphene oxide/sphere-like CoS hierarchical architecture composite as efficient counter electrodes for dye-sensitized solar cells, J. Alloys Comp., 654 (2016) 196–201.

[13] F. Coccia, L. Tonucci, D. Bosco, M. Bressan, N. d'Alessandro, One-pot synthesis of lignin-stabilised platinum and palladium nanoparticles and their catalytic behaviour in oxidation and reduction reactions, Green Chem., 14 (2012) 1073.

[14] J. Ralph, K. Lundquist, G. Brunow, F. Lu, H. Kim, P.F. Schatz, J.M. Marita, R.D. Hatfield, S.A. Ralph, J.H. Christensen, W. Boerjan, Lignins: Natural polymers from oxidative coupling of 4-hydroxyphenyl-propanoids, Phytochem. Rev., 3 (2004) 29–60.

[15] A. Naseem, S. Tabasum, K.M. Zia, M. Zuber, M. Ali, A. Noreen, Lignin-derivatives based polymers, blends and composites: A review, Int. J. Biol. Macromol., 93 (2016) 296–313.

[16] Y. Chang, S. Xing, X. Wei, Y. Wu, Z. Ma, Ligno sulfanate-assistant hydrothermal method for synthesis of titanate nanotubes with improved adsorption capacity for metal ions, Mater. Lett., 132 (2014) 353–356.

[17] W. Liu, R. Zhou, D. Zhou, G. Ding, J.M. Soah, C.Y. Yue, X. Lu, Lignin-assisted direct exfoliation of graphite to graphene in aqueous media and its application in polymer composites, Carbon, 83 (2015) 188–197.

[18] Y. Ge, L. Qin, Z. Li, Lignin microspheres: An effective and recyclable natural polymer-based adsorbent for lead ion removal, Mater. Design, 95 (2016) 141–147.

[19] F.J. Martín-Jimeno, F. Suárez-García, J.I. Paredes, A. Martínez-Alonso, J.M.D. Tascón, Activated carbon xerogels with a cellular morphology derived from hydrothermally carbonized glucose-graphene oxide hybrids and their performance towards CO_2 and dye adsorption, Carbon, 81 (2015) 137–147.

[20] R. Zhang, Q. Qu, B. Han, B. Wang, A novel silica aerogel/porous Y_2SiO_5 ceramics with low thermal conductivity and enhanced mechanical properties prepared by freeze casting and impregnation, Mater. Lett., 175 (2016) 219–222.

[21] Y.S. Ho, G. McKay, Pseudo-second order model for sorption processes, Process Biochem., 34 (1999) 451–465.

[22] S. Lagergren, Zur theorie der sogenannten adsorption geloster stoffe. Kungliga svenska vetenskapsakademiens, Handlingar, 24 (1898) 1–39.

[23] H. Freundlich, Over the adsorption in solution, J. Phys. Chem, 57 (1906) 470.

[24] I. Langmuir, The adsorption of gases on plane surfaces of glass, mica and platinum, J. Amer. Chem. Soc., 40 (1918) 1361–1403.

[25] F. Zhou, J.G. Yu, X.Y. Jiang, 3D porous graphene synthesised using different hydrothermal treatment times for the removal of lead ions from an aqueous solution, Micro Nano Lett., 12 (2017) 308–311.

[26] Z. Li, B. Song, Z. Wu, Z. Lin, Y. Yao, K.-S. Moon, C.P. Wong, 3D porous graphene with ultrahigh surface area for microscale capacitive deionization, Nano Energy, 11 (2015) 711–718.

[27] Q. Li, J.G. Yu, F. Zhou, X.Y. Jiang, Synthesis and characterization of dithiocarbamate carbon nanotubes for the removal of heavy metal ions from aqueous solutions, Colloids Surfaces A: Physicochem. Eng. Asp., 482 (2015) 306–314.